Journal of Materials Chemistry A

Valorisation of Waste to Yield Recyclable Composites of Elemental Sulfur and Lignin

Journal:	*Journal of Materials Chemistry A*
Manuscript ID	TA-ART-03-2019-003222.R1
Article Type:	Paper
Date Submitted by the Author:	19-May-2019
Complete List of Authors:	Karunarathna, Menisha; Clemson University, Department of Chemistry Lauer, Moira; Clemson University, Department of Chemistry Thiounn, Timmy; Clemson University, Department of Chemistry Smith, Rhett; Clemson University, Department of Chemistry Tennyson, Andrew; Clemson University, Department of Chemistry

ARTICLE

Valorisation of Waste to Yield Recyclable Composites of Elemental Sulfur and Lignin

Received 00th June 2018,
Accepted 00th January 20xx

DOI: 10.1039/x0xx00000x

www.rsc.org/

*Menisha S. Karunarathna,[a] Moira K. Lauer,[a] Timmy Thiounn[a], Rhett C. Smith,[*a] and Andrew G. Tennyson[*ab]*

Lignin is the second-most abundant biopolymer in nature and remains a severely underutilized waste product of agriculture and paper production. Sulfur is the most underutilized byproduct of petroleum and natural gas processing industries. On their own, both sulfur and lignin exhibit very poor mechanical properties. In the current work, a strategy for preparing more durable composites of sulfur and lignin, **LS$_x$**, is described. Composites **LS$_x$** were prepared by reaction of allyl lignin with elemental sulfur, whereby some of the sulfur forms polysulfide crosslinks with lignin to yield a three-dimensional network. Even relatively small quantities (<5 wt.%) of the polysulfide-crosslinked lignin network provides up to a 3.4-fold increase in mechanical reinforcement over sulfur alone, as measured by the storage moduli and fexural strength determined from dynamic mechanical analysis (temperatue dependence and stress-strain analysis). Notably, **LS$_x$** composites could be repeatedly remelted and recast after pulverization without loss of mechanical strength. These initial studies suggest potential practical applications of lignin and sulfur waste streams in the ongoing quest towards more sustainable, recyclable structural materials.

Introduction

Lignin and cellulose are the primary components of agricultural waste, of which over five billion metric tons result from pre-consumer processing annually.[1] Paper production produces an additional 600,000 tons/yr of lignin waste.[2] When embedded in a cellulose and hemicellulose composite, lignin (Fig. 1) is responsible for the structural integrity of fibrous plants and thus ultimately of all timber-built structures.[3,4] Despite the structural utility of lignin in naturally-occurring composites and significant motivation to valorise lignin as an element of synthetic materials, it remains underexploited.[1] Another abundant, underutilized by-product of human industry is elemental sulfur. Elemental sulfur (S_8) is produced by the energy sector when natural gas, petroleum and coal are refined to produce cleaner-burning fuels.[5-6] So much by-product sulfur is produced in the refining process that even after industrial sulfur consumption needs have been met, >7 million tons of S_8 are left unused every year,[3,7] spurring significant efforts to exploit it as an affordable component of materials.[8,9] Elemental sulfur itself is quite brittle, yet small quantities of sulfur crosslinking agents improve the structural properties of natural rubber through vulcanization.[10–12] Pyun's group has recently made significant strides to elucidating commercial applications for high sulfur-content materials[6,13–26] that are made by crosslinking bulk elemental sulfur with lower percentages of olefins (Scheme 1) to yield high sulfur-content networks. Such high sulfur-content materials that have proven useful for applications ranging from water purification to battery materials.[47-53] We and other groups have explored similar avenues using other organic crosslinkers.[8,27–29] At STP, sulfur exists as S_8 rings in a morphology referred to as orthorhombic or α-sulfur. Upon heating, sulfur first melts at 120 °C and then undergoes homolytic ring opening at 159 °C to form diradicals. At higher temperatures, these diradicals form

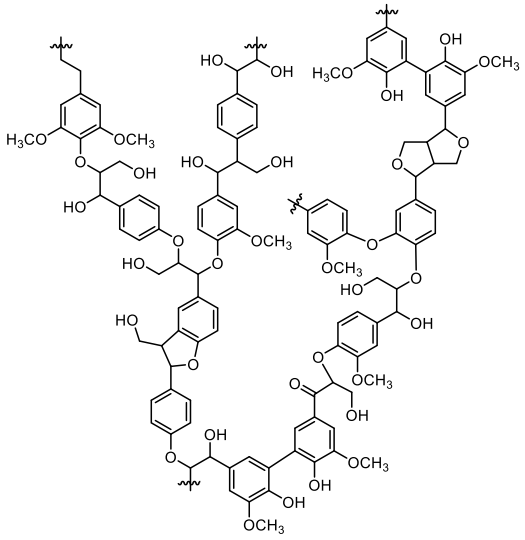

Figure 1. Representative structure of lignin.

[a] *Department of Chemistry , Clemson University, Clemson, South Carolina, 29634, United States*
[b] *Department of Materials Science and Engineering, Clemson University, Clemson, South Carolina, 29634, United States*

†Electronic Supplementary Information (ESI) available: Proton NMR spectral data, FTIR spectra, TGA curves, analysis of char yield versus composition; DSC curves.

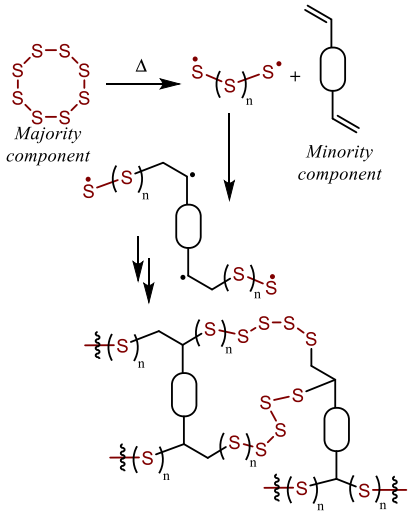

Scheme 1. A generalized scheme for crosslinking olefins with sulfur

polymeric sulfur diradicals. It is these polymeric diradicals that react with olefins to form the crosslinked networks (Scheme 1). We recently demonstrated that materials having reasonable storage moduli and flexural strengths on par with that of Portland cement could be attained by utilizing a cellulose derivative as the organic component for a high sulfur-content composite.[12] This study demonstrated that mechanical improvements could be made to sulfur by crosslinking with a minority fraction of biopolymer: up to a 2-fold improvement in storage modulus at room temperature was accomplished upon crosslinking with 20% of the cellulose derivative. These materials were also thermally healable over many pulverization/recasting processes without loss of strength.

In light of the successful crosslinking of sulfur with cellulose derivative, and on the basis of lignin's ability to provide structural integrity to biocomposites, we hypothesized that we could prepare durable composites of sulfur and lignin. Herein, we report the preparation of composites **LS$_x$** (*x* = percent by mass sulfur in monomer feed, Scheme 2) prepared by reaction of allyl lignin and sulfur, wherein *x* is varied from 80 to 99. The chemical and bulk composition, thermal, morphological and mechanical properties of the materials are discussed.

Results and Discussion

Synthesis and Characterization of Allyl Lignin

The complex, heterogeneous macromolecular structure of lignin (Fig 1)[30] and its low solubility make synthesis and characterization of lignin derivatives challenging.[31–33] In the current context, lignin had to be derivatized with olefinic units to allow reaction with sulfur diradicals.[8, 19, 46] Allyl lignin was prepared by an established method for this study (Scheme 2).[34,35] Analysis of allyl lignin by ^{1}H NMR spectrometry, FT-IR spectroscopy (Fig. S1-2 in the ESI), and elemental analysis match reported data.[36]

Depending on the source (e.g., hardwood, softwood or grassy plants), the relative ratio of the several hydroxyl-bearing functionalities in lignin will vary (Fig. 2, upper). Phosphorus-31 NMR spectrometric techniques are typically used to interrogate these ratios.[34] In this work, the commercial lignin and its allylated derivative were analyzed by first phosphitylating all hydroxyl groups with excess TMDP (Scheme 3) in the presence of HNDI as an internal standard.[35,34] Each of the phosphitylated –OH units has a characteristic shift in the ^{31}P NMR spectrum (Fig. 2, upper). Whereas integrations of typical ^{31}P NMR spectra are not accurate, the integration accuracy in the current context was assured by employing a 10 s pulse delay, 90° pulse angle, and adding chromium (III) acetylacetonate to the samples as a spin relaxation agent. Analysis of spectra so obtained (Fig. 2a) allowed quantification of each type of hydroxyl functionality in the commercial lignin starting material (Table 1), for a total hydroxyl content of 6.0 mmol/g,[37] with relative hydroxyl functionality ratios typical of a softwood lignin.[38]

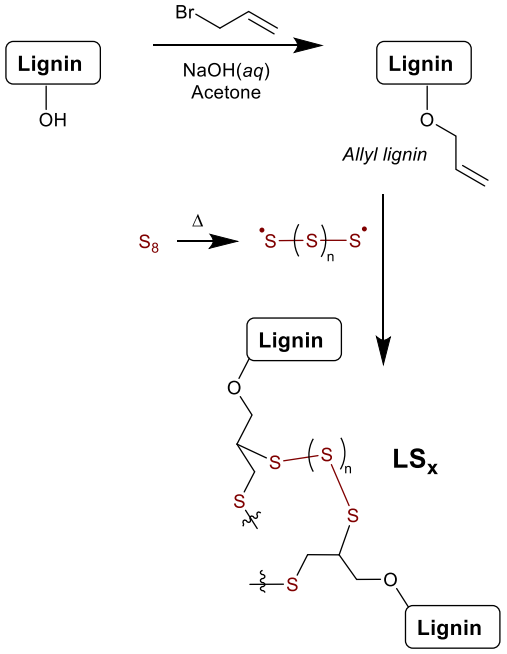

Scheme 2. Synthesis of allyl lignin and **LS$_x$**. Several type of lignin hydroxyl sites are modified by allyl groups in the current work, as delineated in Figure 1 and quantified in Table 1.

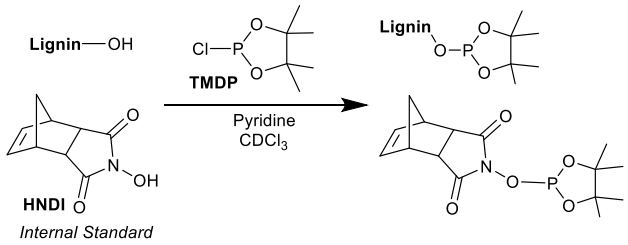

Scheme 3. Phosphitylation of –OH groups in lignin and an internal standard used for quantification by ^{31}P NMR spectrometry. Allyl lignin was treated under identical conditions, whereupon all non-allylated –OH groups were phosphitylated.

In allyl lignin some of the hydroxyl groups are allylated; those sites will not be phosphitylated and so will not contribute to the ^{31}P NMR spectrum. The relative decrease in peak integration for allyl lignin versus lignin spectra allowed for the calculation of percent allylation for each hydroxyl functionality (Table 1). The expected quantitative allylation of phenolic hydroxyl groups was observed, in addition to allylation of 49% of aliphatic alcohol and 72% of carboxylic acid hydroxyl groups. Overall, there are 4.9 mmol of allyl functionalities per gram of material in the allyl lignin used to prepare the **LS$_x$** materials.

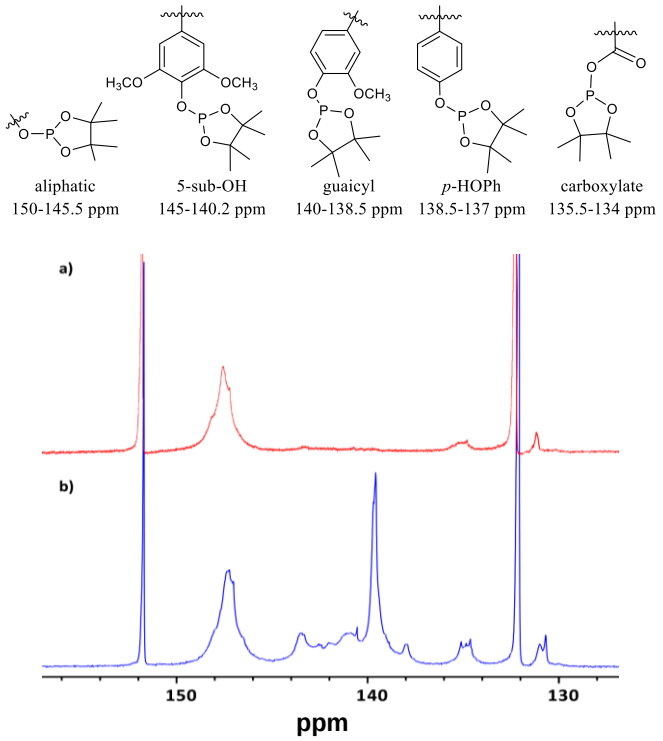

Fig 2. Structures for phosphitylated units in lignin and allyl lignin (upper) and ^{31}P NMR spectra (lower) for a) allyl lignin and b) commercial lignin after phosphitylation.

Table 1 Difference in hydroxyl functionality of allyl lignin and reference lignin sample. Structures for each functionality are provided in Figure 2.

Functionality	Chemical Shift (ppm)	Lignin (mmol/g)	Free OH in Allyl lignin (mmol/g)	% allylated
Carboxylate	134-135.5	0.36	0.10	70
p-HOPh	137-138.5	0.25	–[c]	100
Guaicyl	138.5-140	1.69	–[c]	100
5-Sub–OH	140.2-145	1.61	–[c]	100
Aliphatic	145-150	2.05	1.0	49

[c] No visible peak is observed.

Synthesis and Characterization of Allyl Lignin-Sulfur Materials (LS$_x$)

The reaction of allyl lignin with sulfur was carried out at 180°C, where sulfur exists primarily as polymeric diradicals (Scheme 2),[13] to prepare materials **LS$_x$** (*x* = wt% S_8 in the monomer feed). Materials were prepared wherein sulfur feed ratios ranged from 80-99 wt%. Over the course of the reaction, the mixture changed from the red-orange color characteristic of polymeric sulfur diradicals to the dark brown color of **LS$_x$**. After reaction, the reaction mixture consisted of primarily molten **LS$_x$** and a small fraction of precipitate. While still at 180 °C, the precipitate was separated away from the liquid and the liquid (**LS$_x$**) was retained for further study. When these molten samples of **LS$_x$** were cooled to room temperature, each became a hard, brown, glassy-looking solid. In contrast, when a sample of pure sulfur is treated under the reaction conditions in the absence of an organic crosslinker, the polymeric sulfur that is formed at elevated temperatures reverts back to the brittle, yellow material characteristic of orthorhombic sulfur over about 48 h at room temperature. In sharp contrast, once **LS$_x$** samples are stable for at least nine months without change in physical appearance or deterioration in properties.

Both **LS$_x$** and the reaction precipitate were subjected to elemental microanalysis for C, H, N and S to assess their composition (see Experimental section). This analysis revealed that the precipitate consisted of primarily lignin that had separated, presumably due to poor miscibility of lignin with sulfur. As a result, the lignin content ultimately incorporated into **LS$_x$** materials is somewhat lower than that added to the monomer feed (Table 2).

Table 2 LS$_x$ composition data

Material	Allyl Lignin in monomer feed (wt%)	Allyl Lignin incorporated (wt%)[a]	CS_2-insoluble (wt%)
LS$_{80}$	20	5.0	92
LS$_{85}$	15	3.4	91
LS$_{90}$	10	1.5	87
LS$_{95}$	5	1.0	84
LS$_{99}$	1	0.4	84

[a]Determined from elemental analysis

On the basis of our previous work,[8] it was hypothesized that **LS$_x$** samples could be composites consisting of bulk sulfur that is reinforced by an interpenetrating 3D network. If this were the case, the network would be comprised of allyl lignin crosslinked with oligo- or polysulfide chains as depicted in Scheme 2 and orthorhombic sulfur would fill some of the voids in the network. Free orthorhombic sulfur is highly soluble in CS_2, whereas a highly-crosslinked polymer would not be. In an effort to extract selectively any free orthorhombic sulfur, each **LS$_x$** sample was thus extracted several times with CS_2 until no more mass was extractable. The CS_2-soluble and CS_2-insoluble fractions were separated and analyzed by elemental microanalysis (Table 2). As anticipated, the CS_2-soluble fractions consist of almost

entirely sulfur, whereas lignin and attendant polysulfide crosslink chains are retained in the CS_2-insoluble fractions. The presence of polymeric sulfur was later confirmed by DSC measurements as well (*vide infra*). In lower sulfur-content **LS$_x$** samples (x = 80, 85, 90), up to 92% of the sulfur in the sample is in the polysulfide crosslinked form, with little sulfur present in the orthorhombic form. This is in stark contrast to similarly-prepared materials in which sulfur was crosslinked with 5 wt. % of a polystyrene derivative (twice the wt% of crosslinking agent as in **LS$_{80}$**),[8] wherein only 19% of S was incorporated as polysulfide crosslinks and 81% was orthorhombic. The elemental analysis data for the CS_2-insoluble fraction allowed accurate calculation of the average length of the polysulfide crosslinking chains in **LS$_{80}$** and **LS$_{85}$** to be 48 and 103, respectively. This compares well with some of the reported cellulose-crosslinked sulfur composite, which had polysulfide crosslinks ranging from 20 to 60 sulfur atoms in length.

The fact that **LS$_{80\text{-}90}$** successfully sequesters the majority of sulfur in the polymeric form addresses a key deficiency to which some other high sulfur-content materials are subject. Materials comprising majority orthorhombic sulfur can release sulfur through sublimation or blooming of crystalline sulfur to the surface over time, whereas polymeric sulfur effectively stabilized by a supporting network is not subject to these degradation pathways.

In addition to establishing the presence of polymeric sulfur in **LS$_x$**, direct evidence for C–S bond formation between that polymeric sulfur and the allyl lignin was revealed by IR spectroscopy. Specifically, a peak at 620 cm^{-1}, attributable to C–S stretch,[39] is present in the FT-IR spectrum of each **LS$_x$** sample (Fig. S3 in the ESI). The IR spectra also confirm retention of the characteristic peaks for softwood lignin such as the out-of-plane aromatic C–H deformation (823-875 cm^{-1}), symmetric aryl ring stretching (1594 cm^{-1}), aromatic CH in plane deformation (1028 cm^{-1}) and the methyl/methylene C–H stretches (2952 cm^{-1}).[40] The extraction/elemental analysis studies confirmed the presence of some free sulfur in **LS$_x$**, while IR spectroscopy confirmed both formation of C–S bonds and retention of the basic lignin architecture. Taken together, these data support the characterization of **LS$_x$** as composites comprised primarily of sulfur-crosslinked lignin with some quantity of retained orthorhombic sulfur backfilling available volume in the network.

Table 3 Summary of TGA and DSC data.

Material	T_d (°C)[a]	DSC T_g (°C)	DSC T_m (°C)	ΔH_m J/g	ΔH_{cc} J/g	%xtl[c]
LS$_{80}$	236	−34	118	30	25	8
LS$_{85}$	235	−35	118	34	13	40
LS$_{90}$	237	NA[b]	117	34	NA	67
LS$_{95}$	235	NA[b]	107	37	NA	63
LS$_{99}$	233	NA[b]	113	47	NA	91
S_8	228	NA[b]	120	51	NA	100

[a]T_d was determined by calculating the temperature at which 5% mass was lost. [b]No visible transition in the range studied. [c]percent crystallinity compared to that of sulfur (normalized to 100%).

Thermal Analysis of LS$_x$

The thermal stability of **LS$_x$** samples was assessed by thermogravimetric analysis (TGA, Table 3). The TGA trace for pure sulfur exhibited a single decomposition event with a decomposition temperature (T_d) at 228° C. In contrast, lignin decomposes over a broader temperature range, reflecting the variable stabilities of the diverse functionalities present.[41] The onset of initial lignin decomposition at 201 °C is attributable to degradation of propanoid side chains, while the second decomposition from 360−370 °C is due to cleavage of the β-β and C–C linkages.[41] In **LS$_{90\text{-}99}$** the thermal decomposition is driven by the predominant sulfur component, so all of them exhibit a T_d of 233-237 °C (Fig S4, ESI). These values are similar to those for previously-reported high sulfur-content materials.[17,8] In contrast, a conspicuous two step degradation was observed for **LS$_{80}$** and **LS$_{85}$**, wherein the first decomposition event resembles that of sulfur and a second decomposition step occurs over the range of 355-365 °C, attributed to β-β and C–C linkages cleavage in lignin. The expected increase in char yield (at 800 °C) concomitant with increasing lignin content was also observed (Fig. S5 in the ESI).

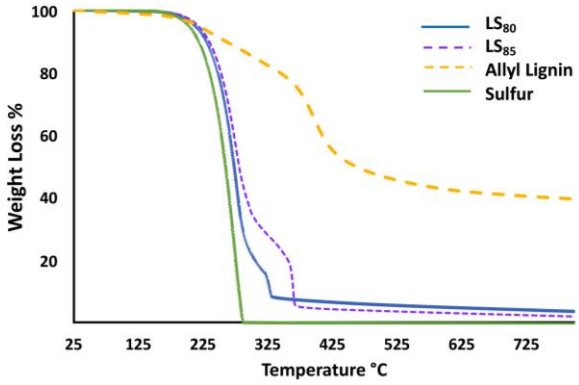

Fig 3. TGA curves of **LS$_{80}$** and **LS$_{85}$** compared with those for sulfur and allyl lignin. DGA (derivative curves) are provided in the ESI Fig. S8.

Differential scanning calorimetry (DSC, Table 3) did not reveal any glass transition (T_g) temperature over the range investigated for the higher sulfur-content composites (**LS$_{99}$**, **LS$_{95}$**, **LS$_{90}$**) or for sulfur alone. That the DSC data for **LS$_{90\text{-}99}$** are nearly identical to that of sulfur is perhaps not surprising, given that they are themselves comprised of 98.5-99.5% sulfur, such that if other transitions are present, they would likely be too small to detect. **LS$_{80}$** and **LS$_{85}$**, however, showed the glass transition for polymeric sulfur at −34 to −35 °C.[42,43] The **LS$_x$** composites also exhibited melt peaks at approximately 106–116 °C, the intensity of which scales with the relative amount of sulfur in the material (Fig. S6 , ESI). DSC analysis of the most-crosslinked **LS$_{80}$** and **LS$_{85}$** samples also show cold

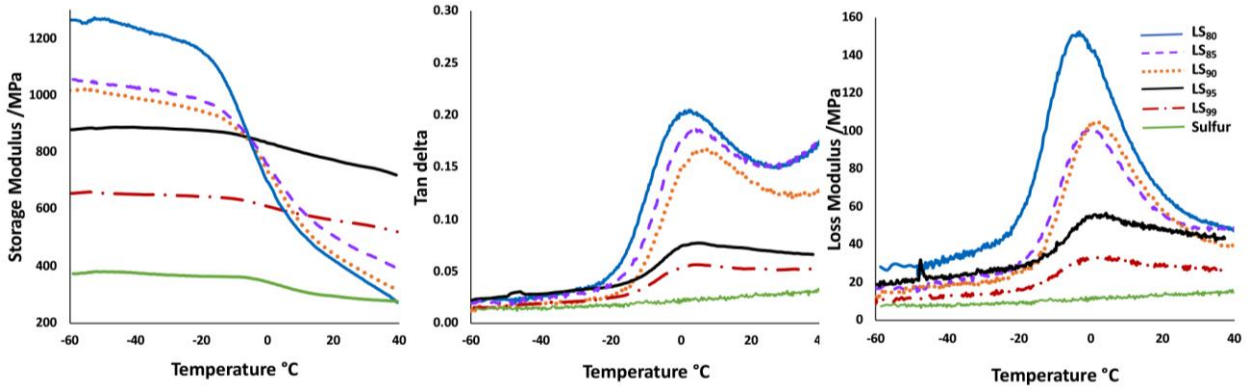

Fig 4. DMA data of **LS$_{80}$** (blue solid line), **LS$_{85}$** (purple dashed line), **LS$_{90}$** (orange dotted line), **LS$_{95}$** (black solid line), **LS$_{99}$** (red dashed line), sulfur (green solid line**) a)** Comparison of storage modulus curves of **LS$_x$** materials. **b)** tan delta curves. **c)** Loss modulus curves.

crystallization peaks. The cold crystallization exotherm reflects partial organization of polymer chains above the glass transition temperature, typical of network-stabilized polymeric sulfur domains.[44]

By comparing the integration of melting and cold crystallization enthalpies of sulfur and **LS$_x$** materials, the relative percent crystallinity of the materials was calculated (the equation for this calculation is provided in the Experimental section and data are summarized in Table 3). The crystallinity of **LS$_{80}$** is only 8% that of pure sulfur. Perhaps more surprisingly, the incorporation of even 1% lignin in **LS$_{95}$** leads to a material only 63% as crystalline as orthorhombic sulfur. The reduction of crystallinity is one feature that results in reduced brittleness of high sulfur-content materials, as elucidated by the DMA measurements discussed below.

Table 4. Summary of DMA data.

Material	E' (−60 °C) (MPa)	tan δ T_g (°C)	E'' T_g (°C)	flexural strength/modulus (MPa)
S_8	373	NA[a]	NA[a]	NA
LS$_{80}$	1265	3.3	−2.5	2.1/87
LS$_{85}$	1049	5.9	−1.2	1.5/76
LS$_{90}$	1016	6.3	0.5	1.7/57
LS$_{95}$	824	NA[a]	NA[a]	ND
LS$_{99}$	656	NA[a]	NA[a]	ND

[a] No visible transition in the range studied.

Mechanical Analysis of LS$_x$

One of the main objectives of this work was to determine the extent to which the incorporation of lignin into sulfur could enhance the mechanical properties of the composite materials. Dynamic Mechanical Analysis (DMA) was thus carried out to assess the viscoelastic properties of the **LS$_x$** samples.

The results of DMA data are summarized in Fig. 4 for the storage moduli (E', Fig. 4a), loss moduli (E'', Fig. 4b) and energy dissipation parameter (tan δ, Fig. 4c) for the five composites and for orthorhombic sulfur. The calculated Flexural strength and the modulus for the strongest materials (**LS$_{80}$**, **LS$_{85}$** and **LS$_{90}$)** are also indicated in the Table 4. The most lignin-reinforced material predictably had the highest storage modulus prior to the glass transition, with steady decrease storage moduli with decreasing lignin percentage. Remarkably, even **LS$_{99}$**,which is comprised by only 0.4% lignin has a ~2-fold greater storage modulus below T_g than does elemental sulfur. The storage moduli data also validate the hypothesis that very little polymeric crosslinking agent is needed to reinforce sulfur as compared to small molecule crosslinking. For example, sulfur/1,3-diisopropenylbenzene (DIB) copolymers having 17.5 wt% DIB crosslinking agent, exhibits a storage modulus of 1000 MPa at −50 °C, on par with that of **LS$_{90}$** in which only 1.5% of the crosslinking agent has been added.[17]

The ability of the **LS$_x$** composites to dissipate energy, as reflected in the intensity of the tan δ curves in Fig. 4C), also scale predictably with the percent of lignin in the sample, with the highest ability to dissipate energy predictably assigned to the most-reinforced **LS$_{80}$** composite. The T_g values obtained from DMA differ from those determined by DSC (Table 4). This is expected because, whereas DSC, T_g values reflect a change in specific heat capacity, the DMA-derived values reflect changes in the coefficient of thermal expansion.[45]

Flexural stress, a combination of tensile and compression stress, are typical challenges to structural materials. The flexural strength and the modulus were thus calculated from stress-strain analysis of **LS$_{80–90}$** (Fig. 5). As expected, the highest flexural strength (2.1 MPa) and modulus were attained for **LS$_{80}$** due to higher stiffness endowed by higher crosslink density. These are fairly good flexural strengths; for comparison, the flexural strength of Portland cement is 3.7 MPa when measured under the same conditions used for the **LS$_x$** materials, though

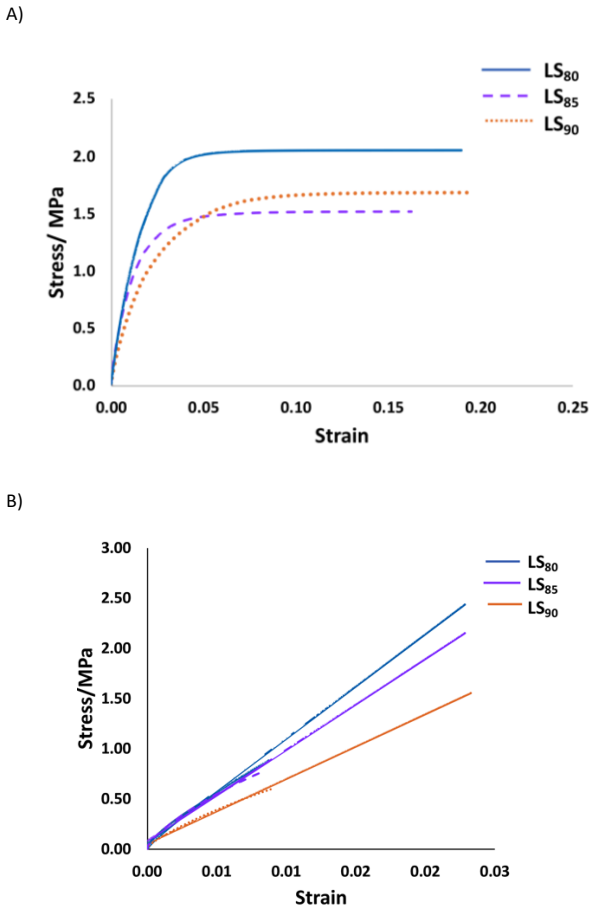

Figure 5. A) Stress-strain curves of **LS$_{80}$** (blue solid line)**LS$_{85}$** (purple dashed line) and **LS$_{90}$** (orange dotted line). Samples broke at the point where each curve ends. B) Inset of the stress-strain curve over the linear region for **LS$_{80}$**.

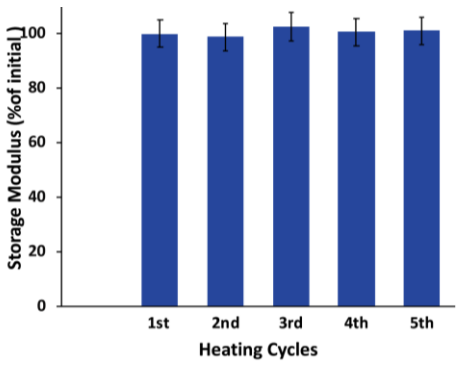

Figure 6. Storage moduli values of LS$_{80}$ at room temperature, over five heating cycles.

Portland cement has a much higher storage modulus at room temperature.

Because S–S bond formation is thermally reversible,[29] materials comprising such bonds are tantalizing targets for thermally-healable and recyclable materials.[8] In order to assess the thermal healability/recyclability of **LS$_{80}$**, the storage modulus (at 25 °C) was measured, then the sample was subjected to several cycles in which it was pulverized into small pieces, reheated at 180 °C in the mold, and then allowed to cure at room temperature. After each cycle, the storage modulus was remeasured. The storage modulus was maintained within experimental error over at least five cycles (Fig. 6).

Conclusions

Softwood lignin biopolymer can be readily modified with allyl groups to allow its reaction with sulfur diradicals. The resultant materials are primarily polysulfide chains that crosslink lignin to form a network. Some free orthorhombic sulfur is still present in these materials that is not covalently attached to the network. The composites, though comprised of ≥95% sulfur by mass, are remarkably stronger than sulfur alone. The composites are also thermally healable, and so can be recast over several cycles without loss of strength. Efforts to improve on the mechanical strength of such biopolymer/sulfur composites is underway.

Conflicts of interest

There are no conflicts to declare

Acknowledgements

Funding for this project from the National Science Foundation (CHE-1708844) is gratefully acknowledged.

Experimental Section

Chemicals and Materials

Alkali lignin and 2-chloro-4,4,5,5,-tetramethyl-1,3,2-dioxaphospholane (TMDP) were purchased from Sigma-Aldrich. Sulfur powder (99.5%), *Endo-N*-hydroxy-5-norbornene-2,3-dicarboximide (HNDI) and chromium (III) acetylacetonate (99.9%) were purchased from Alfa Aesar. Carbon disulfide was obtained from Bean Town Chemical. Acetone, sodium hydroxide (99.5%), dry pyridine, deuterated chloroform and allyl bromide were purchased from Fisher Chemical, VWR Analytical, Acros Organics and Oakwood Chemical, respectively. These chemicals were used without further purification unless otherwise noted.

General Considerations

All NMR spectra were recorded on a Bruker Avance spectrometer operating at 300 MHz for protons and 121.4 MHz for ^{31}P NMR. In order to obtain accurate quantitative integrations from ^{31}P NMR spectra, a 10 s pulse delay and 90° pulse angle were employed and chromium (III) acetylacetonate was added as a spin relaxation agent following the established procedure.[35-34] Thermogravimetric analysis (TGA) data were recorded on a Mettler Toledo TA SDT Q600 instrument over the range 20 to 800 °C, with a heating rate of 2 °C min^{-1} under a flow of N_2 (100 mL min^{-1}). Differential scanning calorimetry (DSC)

data were acquired using a Mettler Toledo DSC 3 STAR^e System over the range of –60 to 140 °C, with a heating rate of 10 °C min^{-1} under a flow of N_2 (200 mL min^{-1}). Each DSC measurement was carried out over three heat-cool cycles, and data are reported for the third cycle. The change in crystallinity between sulfur and the composites was calculated from DSC data using the following equation:

$$\Delta\chi_c = 1 - \left\{\frac{\Delta H_{m(LS_x)} - \Delta H_{cc(LS_x)}}{\Delta H_{m(S)} - \Delta H_{cc(S)}}\right\} * 100\%$$

$\Delta\chi_c$ - Change of percentage crystallinity with respect to sulfur
$\Delta H_{m(LS_x)}$ - Melting enthalpy of composite materials (LS_x)
$\Delta H_{cc(LS_x)}$ - Cold crystallization enthalpy of composite materials (LS_x)
$\Delta H_{m(S)}$ - Melting enthalpy of sulfur
$\Delta H_{cc(S)}$ - Cold crystallization enthalpy of sulfur

Dynamic Mechanical Analysis (DMA) was performed using a Mettler Toledo DMA 1 STAR^e System in single cantilever mode. DMA samples cured for 120 h were cast from silicone resin molds (Smooth-On Oomoo® 30 tin-cure). The sample dimensions were 1.5 × 8 × 23 mm. The clamping force was 1 cN·m and the temperature range was –60 to 40 °C with a heating rate of 2 °C min^{-1}. The measurement mode was set to displacement control with a displacement amplitude of 5 µm and a frequency of 1 Hz. Samples were cured for 120 h prior to stress-strain analysis at ambient conditions with the DMA instrument operating in single cantilever mode. The force was varied from 0 to 7 N with a ramp rate of 0.1 N·min^{-1}. Fourier transform infrared spectra were obtained using a Shimadzu IR Affinity-1S instrument operating over the range of 400-4000 cm^{-1} at ambient temperature using an ATR attachment.

Allylation of Lignin

This procedure is based on literature precedent.[34,35] Lignin 20 g was dissolved in 800 mL of 0.5 *M* NaOH(*aq*)/acetone (1:3). Allyl bromide (40 g, 0.33 mol) was added and the mixture was allowed to heat for 5 hours at 40° C with continuous stirring. After 5 hours, the solution was concentrated under reduced pressure using a rotary evaporator. The remaining solution was acidified to pH 2 by dropwise addition of concentrated HCl(*aq*), resulting in the formation of a precipitate. The precipitate was collected by vacuum filtration followed by four consecutive washes with distilled water and then with hexanes. The final product was vacuum dried for 24 hours at 40° C.

Phosphitylation Reaction

Phosphitylation of lignin was performed with TMDP in pyridine and $CDCl_3$ (1.6/1.0, v/v), according to a known method.[35,34] HNDI (HNDI, 121.5 mM, $CDCl_3$/pyridine 4.5:0.5) was used as the internal standard while chromium (III) acetylacetonate (1 mg/mL) was used as the relaxation agent. The reaction was carried out in a glove box in order to prevent the interference of moisture.

General synthesis of LS_x (*x* = wt% sulfur in monomer feed)

Elemental sulfur was weighed directly into a glass vial. The vial was heated to 180 °C in an oil bath over which time the sulfur melted. Once the sulfur turned a viscous dark red-orange color (indicative of thermal ring-opening), the appropriate amount of allyl lignin was slowly added to the molten sulfur. Following addition, heating was continued for 48 h with continuous stirring with a magnetic stir bar. This general synthesis was used to synthesize **LS_{99}**, **LS_{95}**, **LS_{90}, LS_{85}** and **LS_{80}** Each of the lignin-sulfur combinations (composite materials) was subjected to elemental combustion microanalysis.

CAUTION: Heating elemental sulfur with organics can result in the formation of H_2S gas. H_2S is toxic, foul-smelling, and corrosive.

Notes and references

1 C. Wang, S. S. Kelley and R. A. Venditti, *ChemSusChem*, 2016, **9**, 770–783.
2 L. Zoia, A. Salanti, P. Frigerio and M. Orlandi, *BioResources*, 2014, **9**, 6540–6561.
3 L. Silvestroni, *Topics in Current Chemistry, Biochemistry*, 1980, vol. 7.
4 R. Ma, Y. Xu and X. Zhang, *ChemSusChem*, 2015, **8**, 24–51.
5 X. Zhang, Y. Tang, S. Qu, J. Da and Z. Hao, *ACS Catal.*, 2015, **5**, 1053–1067.
6 J. Lim, J. Pyun and K. Char, *Angew. Chemie Int. Ed.*, 2015, **54**, 3249–3258.
7 R. Steudel and B. Eckert, *Elemental sulfur and sulfur-rich compounds II*, Springer Science & Business Media, 2003, vol. 2.
8 T. Thiounn, M. Lauer, M. S. Bedford, R. C. Smith and A. G. Tennyson, *RSC Adv.*, , DOI:10.3133/70180197,.
9 M. P. Crockett, A. M. Evans, M. J. H. Worthington, I. S. Albuquerque, A. D. Slattery, C. T. Gibson, J. A. Campbell, D. A. Lewis, G. J. L. Bernardes and J. M. Chalker, *Angew. Chem. Int. Ed. Engl.*, 2016, **55**, 1714–1718.
10 C. Goodyear, 1844, US3633A.
11 E. H. Farmer and F. W. Shipley, *J. Chem. Soc.*, 1947, 1519–1532.
12 Lauer M.K, Estrada-Mendoza T.A, McMillen C.D, Chumanov G, Tennyson A.G, Smith R.C. *Durable, Remeltable Materials from Agricultural and Petrochemical Wastes*, 2019. Submitted for publication.
13 W. J. Chung, J. J. Griebel, E. T. Kim, H. Yoon, A. G. Simmonds, H. J. Ji, P. T. Dirlam, R. S. Glass, J. J. Wie, N. A. Nguyen, B. W. Guralnick, J. Park, Á. Somogyi, P. Theato, M. E. Mackay, Y. E. Sung, K. Char and J. Pyun, *Nat. Chem.*, 2013, **5**, 518–524.
14 Y. Zhang, K. M. Konopka, R. S. Glass, K. Char and J. Pyun, *Polym. Chem.*, 2017, **8**, 5167–5173.
15 J. J. Griebel, *Namnabat, LE Anderson, RS Glas. RA Norwood, ME Mackay, K. Char, J. Pyun, ACS Macro Lett*, 2015, **4**, 862–866.
16 J. J. Griebel, G. Li, R. S. Glass, K. Char and J. Pyun, *J. Polym. Sci. Part A Polym. Chem.*, 2015, **53**, 173–177.
17 S. Diez, A. Hoefling, P. Theato and W. Pauer, *Polymers (Basel).*, 2017, **9**, 1–16.
18 P. T. Dirlam, A. G. Simmonds, T. S. Kleine, N. A. Nguyen, L. E. Anderson, A. O. Klever, A. Florian, P. J. Costanzo, P. Theato and M. E. Mackay, *Rsc Adv.*, 2015, **5**, 24718–24722.

19 Y. Zhang, J. J. Griebel, P. T. Dirlam, N. A. Nguyen, R. S. Glass, M. E. Mackay, K. Char and J. Pyun, *J. Polym. Sci. Part A Polym. Chem.*, 2017, **55**, 107–116.
20 J. Park, E. T. Kim, C. Kim, J. Pyun, H. Jang, J. Shin, J. W. Choi, K. Char and Y. Sung, *Adv. Energy Mater.*, 2017, **7**, 1700074.
21 V. P. Oleshko, A. A. Herzing, C. L. Soles, J. J. Griebel, W. J. Chung, A. G. Simmonds and J. Pyun, *Microsc. Microanal.*, 2016, **22**, 1198–1221.
22 V. P. Oleshko, A. A. Herzing, K. A. Twedt, J. J. Griebel, J. J. McClelland, J. Pyun and C. L. Soles, *Langmuir*, 2017, **33**, 9361–9377.
23 J. Lim, U. Jung, W. T. Joe, E. T. Kim, J. Pyun and K. Char, *Macromol. Rapid Commun.*, 2015, **36**, 1103–1107.
24 E. T. Kim, W. J. Chung, J. Lim, P. Johe, R. S. Glass, J. Pyun and K. Char, *Polym. Chem.*, 2014, **5**, 3617–3623.
25 E. T. Kim, J. Park, C. Kim, A. G. Simmonds, Y.-E. Sung, J. Pyun and K. Char, *ACS Macro Lett.*, 2016, **5**, 471–475.
26 J. J. Griebel, N. A. Nguyen, A. V Astashkin, R. S. Glass, M. E. Mackay, K. Char and J. Pyun, *ACS Macro Lett.*, 2014, **3**, 1258–1261.
27 A. . Joyce, *U.S. Geol. Surv.*, 2017, 202.
28 M. J. H. Worthington, R. L. Kucera and J. M. Chalker, *Green Chem.*, 2017, **19**, 2748–2761.
29 F. García and M. M. J. Smulders, *J. Polym. Sci. Part A Polym. Chem.*, 2016, **54**, 3551–3577.
30 K. M. Holtman, H. M. Chang, H. Jameel and J. F. Kadla, *J. Wood Chem. Technol.*, 2006, **26**, 21–34.
31 A. M. Socha, R. Parthasarathi, J. Shi, S. Pattathil, D. Whyte, M. Bergeron, A. George, K. Tran, V. Stavila, S. Venkatachalam, M. G. Hahn, B. A. Simmons and S. Singh, *Proc. Natl. Acad. Sci. U. S. A.*, 2014, **111**, E3587–E3595.
32 A. M. Socha, S. P. Plummer, V. Stavila, B. A. Simmons and S. Singh, *Biotechnol. Biofuels*, 2013, **6**, 61.
33 N. Sun, R. Parthasarathi, A. M. Socha, J. Shi, S. Zhang, V. Stavila, K. L. Sale, B. A. Simmons and S. Singh, *Green Chem.*, 2014, **16**, 2546–2557.
34 D. S. Argyropoulos, *J. Wood Chem. Technol.*, 1994, **14**, 45–63.
35 A. Granata and D. S. Argyropoulos, *J. Agric. Food Chem.*, 1995, **43**, 1538–1544.
36 M. Jawerth, M. Johansson, S. Lundmark, C. Gioia and M. Lawoko, *ACS Sustain. Chem. Eng.*, 2017, **5**, 10918–10925.
37 M. Balakshin and E. Capanema, *J. Wood Chem. Technol.*, 2015, **35**, 220–237.
38 M. Fox, S. C. Fox and A. G. Mcdonald, *Lignin characterization*, 2010, vol. 5.
39 K. K. Jena and S. M. Alhassan, *J. Appl. Polym. Sci.*, 2016, **133**, 1–14.
40 N. M. Stark, D. J. Yelle and U. P. Agarwal, *Lignin Polym. Compos.*, 2015, 49–66.
41 M. Brebu and C. Vasile, *THERMAL DEGRADATION OF LIGNIN-A REVIEW*, 2010, vol. 44.
42 A. M. Zaper and J. L. Koenig, *Makromol. Chem.*, 1988, **1251**, 1239–1251.
43 K. Bandzierz, L. Reuvekamp, J. Dryzek, W. Dierkes, A. Blume and D. Bielinski, *Materials (Basel).*, DOI:10.3390/MA9070607.
44 A. Smith and W. B. Holmes, *J. Am. Chem. Soc.*, 1905, **27**, 979–1013.
45 K. P. Menard, *Dynamic mechanical analysis: a practical introduction*, CRC press, 2008.
46 A. Ahmed and L. P. Blanchard, *Journal of Applied Polymer Science*, 1984, **29**, 1225-1239.
47 Y. Wang and W. Wang, *International Journal of Electrochemical Science*, 2017, **12**, 11929-11941.
48 J. Cheng, Y. Pan, J. Zhu, Z. Li, J. Pan and Z. Ma, *Journal of Power Sources*, 2014, **257**, 192-197.
49 J. X. Zhang, Z. S. Ma, J. J. Cheng, Y. Wang, C. Wu, Y. Pan and C. Lu, *Journal of Electroanalytical Chemistry*, 2015, **738**, 184-187.
50 J.-H. Kim, Y.-H. Lee, S.-J. Cho, J.-G. Gwon, H.-J. Cho, M. Jang, S.-Y. Lee and S.-Y. Lee, *Energy & Environmental Science*, 2019, **12**, 177-186.
51 M. Mann, J. E. Kruger, F. Andari, J. McErlean, J. R. Gascooke, J. A. Smith, M. J. H. Worthington, C. C. C. McKinley, J. A. Campbell, D. A. Lewis, T. Hasell, M. V. Perkins and J. M. Chalker, *Organic & Biomolecular Chemistry*, 2019, **17**, 1929-1936.
52 T. Hasell, D. J. Parker, H. A. Jones, T. McAllister and S. M. Howdle, *Chemical Communications (Cambridge, United Kingdom)*, 2016, **52**, 5383-5386.
53 M. P. Crockett, A. M. Evans, M. J. H. Worthington, I. S. Albuquerque, A. D. Slattery, C. T. Gibson, J. A. Campbell, D. A. Lewis, G. J. L. Bernardes and J. M. Chalker, *Angew. Chem., Int. Ed.*, 2016, **55**, 1714-1718.

